Journal of Catalysis 281 (2011) 156–168

Contents lists available at ScienceDirect

Journal of Catalysis

journal homepage: www.elsevier.com/locate/jcat

Photocatalytic degradation of organic molecules on mesoporous visible-light-active Sn(II)-doped titania

Venkata Bharat Ram Boppana, Raul F. Lobo *

Center for Catalytic Science and Technology, Department of Chemical Engineering, University of Delaware, Newark, DE 19716, USA

ARTICLE INFO

Article history:
Received 4 March 2011
Revised 19 April 2011
Accepted 21 April 2011
Available online 25 May 2011

Keywords:
Photocatalysis
TiO_2
Visible light
Rhodamine B
Cresol
Doping
Anatase
Rutile

ABSTRACT

We report the first demonstration of visible light photocatalytic activity of Sn^{2+}-doped TiO_2. The catalysts are prepared from the reaction of titanium butoxide and several tin precursors at 80 °C in aqueous solutions. Samples synthesized with $SnCl_2$ have lower band gaps (red-shifted to the visible region) with respect to anatase TiO_2. The catalysts are isostructural to anatase TiO_2 even at the highest loadings of Sn^{2+}. When the precursor is changed to $SnCl_4$, rutile is the predominant phase obtained but no reduction in the band gap is observed. The materials are investigated using X-ray diffraction, ultraviolet–visible diffuse reflectance spectroscopy, X-ray photoelectron spectroscopy, IR spectroscopy, photoluminescence, Raman spectroscopy, and other techniques. The majority of surface cation sites are tin, with a fraction of tin also incorporated in the bulk particles. The experiments also indicate the presence of chlorine in the samples, also influencing the optical and catalytic properties as confirmed by comparison to materials prepared using bromide precursors. These catalysts are photocatalytically active for the degradation of organic molecules with rates higher than the standards (P25 TiO_2) and also evidenced from the generation of hydroxyl radicals using visible light. This protocol could be extended to incorporate Sn^{2+} into other oxide semiconductors to prepare photocatalysts with interesting electronic properties. The analysis of the degradation of rhodamine B dye by a de-ethylation mechanism using multivariate chemometric methods is also described.

1. Introduction

The development of photocatalysts that maximize the utilization of sunlight (comprised of 40% visible light) is the aim of many recent reports that investigate photon-driven reactions such as water splitting or degradation of organic compounds [1]. TiO_2 has been studied extensively and is established for some of these applications since the discovery of water splitting by Fujishima and Honda [2]. The advantages of TiO_2 are that it is non-toxic, is inexpensive, and has considerable photostability; still, TiO_2 has a wide band gap of 3.2 eV (420 nm) and cannot utilize visible light efficiently. To offset this drawback, various groups have tried multiple approaches to increase the absorption edge to the visible region [3].

Doping of TiO_2 can be accomplished via introduction of anions or cations. Since the seminal work by Asahi [4] on N-doped TiO_2 for photocatalytic oxidation of dyes and acetaldehyde in visible light, other non-metal dopants like halogens, sulfur, carbon, and phosphorous have been developed and tested. The specific effect of each dopant on the electronic structure is actively debated due to the inability of quantum chemical calculations to predict band edges accurately and due to a range of preparation procedures leading to multiple dopant states in different samples of nominally the same composition. Nonetheless, the introduction of these dopants clearly enhances visible light activity. The effects of metal dopants have also been investigated; for instance, V- and Cr-doped TiO_2 are known to show visible light absorption [5]. Metal doping is fraught with experimental variability as, for example, Cr-doped TiO_2 prepared using impregnation results in only a shoulder in the visible region, whereas Cr introduced by ion implantation leads to a prominent shift in the absorption edge to visible region [3,6]. Thus, no matter what the dopant is, careful experimental analysis using multiple characterization techniques is necessary to clearly understand the structure of modified titania.

Typically, metal-modified titania shows little or no visible light activity as the new states are below the conduction band and act as electron traps [3,7]. Cations that modify the valence band are rare but do improve the oxidative power of holes due to the introduction of new s orbitals near the HOMO, as has been noted for $BiVO_4$ and $CaBi_2O_4$ (Bi^{3+}-6s) [8,9]. Accordingly, the presence of Sn^{2+}-5s orbitals should lead to improved photocatalytic properties as observed by Hosogi et al. [10,11] for Sn^{2+} tantalates and niobates. Here, we investigate this principle by preparing and investigating the photocatalytic properties of tin-doped titania. Sn-doped TiO_2

* Corresponding author. Fax: +1 302 831 1048.
E-mail address: lobo@udel.edu (R.F. Lobo).

0021-9517/$ - see front matter © 2011 Elsevier Inc. All rights reserved.
doi:10.1016/j.jcat.2011.04.014

has been studied earlier (see Table 1), though mostly with Sn^{4+} precursors [12–16]. Fresno et al. [17,18] have investigated the location of Sn^{4+} in TiO_2 synthesized using a variety of precursors. These materials show enhanced photocatalytic activities—although only in the UV region—compared with Degussa P25-TiO_2. Their results and other reports have established no effect [19] or a slight blue-shift [14,20,21] of the band gaps of titania from the introduction of Sn^{4+}, though slight reductions in the band gaps were also observed by other experimental [15,16] (still above 2.99 eV) and theoretical [20,21] results at low tin contents (note that the band gap of SnO_2 is 3.6 eV). In spite of these contradictions – which could arise from different locations of tin and/or the interplay of multiple titania polymorphs – no visible light activity has been observed except by two groups [22,23] who have attributed the activity to a Sn^{4+} 5s level below the conduction band (a mid-gap state) [20,23]. Despite a number of reports on Sn(IV)–TiO_2 (Table 1), important issues like the origin of the absorption spectra, the location and type of the tin dopants (on the surface and in the bulk), and the effect of co-dopants, if any, have not been clearly elucidated. These details could explain the variability in electronic properties reported in the literature (Table 1). To the best of our knowledge, no investigations have been conducted on the effects of Sn^{2+} (5s orbitals) with titania and its visible light photocatalytic activity.

In this report, mesoporous tin-doped titania catalysts (anatase and rutile polymorphs) were synthesized [24] using titanium butoxide as the titanium precursor. A number of tin sources ($SnCl_2$, $SnCl_4$, $SnBr_2$ and $SnBr_4$) were chosen to study the effects of tin precursors. When Sn(II) precursors are employed, the absorption edge of the spectrum of the solid product is red-shifted to the visible region, whilst this was not the case when Sn(IV) precursors were employed. The catalysts' structural and electronic properties were investigated using X-ray diffraction (XRD), Raman spectroscopy, N_2 adsorption isotherms, ultraviolet–visible diffuse reflectance spectroscopy (UV–vis), scanning electron microscopy (SEM), X-ray photoelectron spectroscopy (XPS), infra red spectroscopy (IR), and photoluminescence (PL) measurements. The photocatalytic activities were investigated using rhodamine B (RhB) and cresol as model compounds in UV and visible light conditions after initially verifying the generation of hydroxyl radicals. This report demonstrates the visible light photocatalytic activities of Sn^{2+}-doped titania. Other useful photocatalysts could be prepared from the incorporation of Sn 5s orbitals in d^0 or d^{10} oxides.

2. Experimental

2.1. Synthesis

Sn^{2+}-doped TiO_2 particles are synthesized by the procedure developed by Ghosh et al. [24] from $SnCl_2$. Other protocols using the same precursor resulted in no desirable red-shift in the band gap [25–27]. Titanium butoxide (2 g, Sigma Aldrich, USA) was initially dissolved in anhydrous ethanol (20 ml, Fisher Scientific, USA) and stirred at room temperature. This solution was added to a second solution of $SnCl_2$ (Sigma Aldrich, USA) dissolved in 20 ml deionized (DI) water pre-heated to 80–90 °C [24]. The resulting solution was stirred while maintained at this temperature for an hour. The product was obtained after the solution was centrifuged, washed multiple times with DI water, and dried overnight at 80 °C. The Ti/Sn ratio was changed (5, 9, 20 and 50) to establish the effects of tin loading. The solid products were yellow. To analyze the effects of the precursors, the Ti/Sn content was fixed at 9 and the tin source employed was changed from $SnCl_2$ to $SnCl_4$, $SnBr_2$, and $SnBr_4$ (Sigma Aldrich and Strem Chemicals, USA). White products were obtained when using Sn(IV) precursors. By heating the Sn(II)-synthesized samples (with Ti/Sn = 9) in air at 300 °C for 5 h at a heating ramp 5 °C/min, the previously yellow solid powder turned also white. This latter sample is denoted as the *calcined* product.

2.2. Analytical

Powder X-ray diffraction (XRD) patterns were collected on a Philips X'pert diffractometer using a Cu Kα source. The patterns were obtained from 5 to 70° 2-θ using a step size of 0.02° and 2.5 s per step. The coherence length (or crystallite size) reported here corresponds to the particle size calculated using the full-

Table 1
The properties of Sn–TiO_2 catalysts reported in literature.

Reference	Sn source (if experimental)	Sn content	TiO_2 polymorph	Band gap variation with Sn	Photocatalysis light conditions
[12]	$SnCl_4$	Ti/Sn 4 to 39	Anatase (low Sn) and with rutile (high Sn)	All blue-shift wrt undoped sample (more with low Sn sample)	UV
[13]	$SnCl_4$	1–5 mol%	Anatase + rutile (rutile fraction growing with Sn)	Red-shifted to visible with Sn	UV
[14]	$SnCl_4$	Ti/Sn 9 to 39	Rutile	Blue-shift due to inc. in the CB	UV
[15]	SnO_2	Ti/Sn 9 to 99	Rutile	Decreases initially (till 49, 2.99 eV) then increases (3.04 eV)	–
[16]	$Sn(OAc)_4$	Ti/Sn 2 to 20	Anatase + rutile (rutile fraction growing with Sn)	Decrease till 5, then increases but all above 3 eV	–
[18]	Ph_3SnOH	5–8 atomic %	Variable depending on procedure	No effect	UV
[19]	DFT	1 mol%	Anatase	No effect	–
[20]	DFT	2–4.2 atomic%	Anatase + rutile	R (Sn for Ti) reduces the band gap, but then increases with higher tin. R (Sn for O) and A (Sn for Ti) raises the band gap.	–
[21]	DFT	Ti/Sn 0 to ∞	Rutile	Increases with increase in Sn content	–
[22]	$SnCl_4$	–	Anatase	Red-shifts to the visible region	UV and vis
[23]	$SnCl_4$	Ti/Sn 14.3	Anatase	A new band 0.4 eV below the CB	UV and vis
[25]	$SnCl_2$	–	Anatase + rutile	No red-shift	UV
[26]	SnF_2	Ti/Sn 0 to ∞	Rutile	Increase with Sn content and all above 3 eV	UV
[27]	$SnCl_2$	Sn 0.09 to 0.23 atomic %	Anatase + rutile (rutile fraction growing with Sn)	Decreases from 3.35 eV (no Sn) to 3.07 (0.09 wt.%) then increases to 3.14 eV (0.23 wt.%)	–
[34]	SnF_4	Ti/Sn 1.7 to 15.7	Anatase to Rutile with Sn	3.22 eV (no Sn), 3.35 eV(A, 15.7), 3.08 eV (R, 7.3)	–
[70]	$SnCl_4{\cdot}5H_2O$	Ti/Sn 9 to 99	Anatase (low Sn) and with rutile (high Sn)	All above 3 eV	UV
[71]	$SnCl_4$	Ti/Sn 0.11–19	Rutile	–	–

width half maximum (FWHM) of the (200) diffraction peak at ~47.5° 2-θ. UV–vis spectra were obtained on a Jasco V-550 spectrometer equipped with an ISV-469 integrating sphere from 850 to 220 nm with a bandwidth of 1 nm and using MgO as a reference material. Photoluminescence (PL) experiments from 350 to 600 nm were conducted in a Hitachi F4500 fluorometer fitted with a solid sample holder with an excitation wavelength of 310 nm at a scan speed of 60 nm min^{-1}, response of 0.1 s, excitation and emission slit width of 5 nm. Infra red (IR) measurements were conducted using a Thermo Nicolet Nexus 470 FT-IR in the transmission mode from 4000 to 1100 cm^{-1} using CaF_2 windows; the samples were initially heated in situ in vacuum to ~200 °C to remove adsorbed water. Adsorption isotherms were collected on a Micromeritics ASAP 2010 using N_2 as the adsorbate at 77 K. Prior to the adsorption experiment, the samples were degassed at 120 °C for 5 h. Scanning electron microscopy (SEM) images were obtained on a JEOL JSM7400F microscope with a field emission gun. The imaging using the SEM and elemental analysis using energy dispersive analysis (EDAX) were obtained at a voltage of 3 kV and 15 kV (emission current 10 μA), respectively. Raman spectra were measured using a 100 mW Neon laser using a 532-nm light source. The Raman spectra were collected in the range of 80–1530 cm^{-1} using 3–5 cm^{-1} step size, 20× objective, 50 × 1000 μm^2 aperture, and integration time of 60 s with 2 co-additions. X-ray photoelectron spectroscopy (XPS) measurements were measured with an Al X-ray source with the neutralizer switched on at 100 eV energy and 25 mA of current to reduce sample charging. The survey scan parameters are 1.6 eV/step, 100 ms/step, and pass energy of 187.85 eV in 15 min. The multiscans were done for Sn $3d_{5/2}$, Ti $2p_{3/2}$, O 1s, and C 1s with the following parameters: 0.125 eV $step^{-1}$, 50 ms $step^{-1}$, and 58.7 eV pass energy and 3 sweeps in 240 min. The depth profile Ti/Sn ratio was obtained after sputtering the Ti/Sn = 9 sample with an Ar gun for 3 cycles (10 s/cycle) in an Auger emission spectroscopy (AES) equipment. Charging was minimized by focusing the beam over a larger cross-section of the catalyst. P25 (Degussa) and anatase (Sigma–Aldrich) TiO_2 were used as obtained for comparative purposes.

The general power law derived by Davis and Mott [28] was used to determine the band gap energies (see Fig. S13 in the supporting information section). The equation is;

$$\alpha\hbar\omega \propto (h\nu - E_g)^n \quad (1)$$

where α is the absorption coefficient in Kubelka–Munk $F(R_\infty)$ units, $h\nu$ is the photon energy, E_g is the band gap of the material, and direct allowed transitions ($n = 0.5$) are assumed since this gives the best linear fit [29] when plotting $[F(R_\infty)\, h\nu]^2$ versus photon energy ($h\nu$).

Chemometric methods were applied to analyze and understand the concentration profiles of the de-ethylated intermediates during the photodecolorization of RhB dye. This was done utilizing the multivariate curve resolution–alternating least squares (MCR–ALS) algorithm [30]. The time series data were initially tabulated with the rows and columns representing the absorbance changes with respect to wavelength and time, respectively, and the command line program run in MATLAB [31]. The method consists of bi-linear decomposition of the above described data matrix (D) into temporal concentration profiles (C) and pure species (S) with E representing the residuals, Eq. (2). For RhB decolorization, we assumed the presence of 2 components, RhB (with $\lambda = 554$ nm) and rhodamine (with $\lambda = 497$ nm), and the resultant pure species profiles are similar to the data experimentally observed supporting the physical underpinnings of the deconvolution procedure. The temporal profiles of any additional de-ethylated compounds were found to be insignificant.

$$D = CS^T + E \quad (2)$$

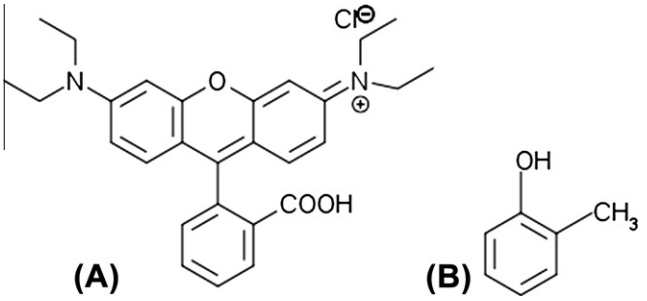

Scheme 1. Organic molecules (rhodamine B and o-cresol) chosen for photocatalytic degradation studies.

2.3. Photocatalytic measurements

Photocatalytic experiments (catalyst loading of 1 g/l) were conducted using rhodamine B (RhB, 5 mg/l) and cresol (100 mg/l) as model compounds (Scheme 1). Details of the experimental setup are in our previous publication [32]. The solutions were initially stirred in the dark for an hour to achieve adsorption–desorption equilibrium after which the photo-reactor light source (450 W Oriel xenon lamp) was turned on. To obtain visible light conditions, a 420-nm Oriel sorting filter was used to block UV radiation. The centrifuged solutions were evaluated for the degradation of the dye in a Jasco V-550 UV–vis spectrometer using the following equation;

$$\eta = 1 - (c/c_0) = 1 - (A/A_0) \quad (3)$$

where η is the degradation, c and A are the concentration and absorbance (554 nm for RhB and 272 nm for cresol) at a particular time during the photocatalytic experiment, and c_0 and A_0 are the initial concentration and absorbance before the start of dark adsorption (at $t = -60$ min). Appropriate control experiments were conducted with the reactant molecules, in UV light with no catalyst and with catalyst in dark; these results are presented in the supporting information and conclusively show that these Sn–TiO_2 samples can be utilized as effective photocatalysts under UV and visible light irradiation.

The amount of hydroxyl radicals was quantified by following the intensity of the molecule 2-hydroxy terephthalic acid. To a 50 ml solution of terephthalic acid (5 mM) and 0.01 M NaOH, 50 mg of the catalyst (Ti/Sn = 9) was added. Upon illumination using visible light, the generated hydroxyl radicals from the presence of the photocatalyst react with terephthalic acid to form 2-hydroxy terephthalic acid. In intervals of 1 h, 3 ml of the solution was pipetted out and the concentration was followed by analyzing its PL band at 425 nm [33].

3. Results

3.1. Catalyst characterization

Incorporation of tin from $SnCl_2$ precursor leads to the formation of the anatase polymorph of TiO_2 irrespective of the tin loading (Fig. 1a) and leads to changes in the absorption spectrum edge that is red-shifted to the visible region. The crystallites are 5–6 nm long as determined using the Scherrer equation (Table 2). One of the Sn^{2+}-doped catalysts (with Ti/Sn = 9) was calcined in air; this sample retains the anatase crystal structure but the band gap increased to 3.23 eV (in the UV region) [24]. When the source of Sn was changed to $SnCl_4$, the product observed is predominantly the rutile titania polymorph. Previous reports [12,16,34] on the incorporation of Sn^{4+} into TiO_2 have shown that anatase is obtained at

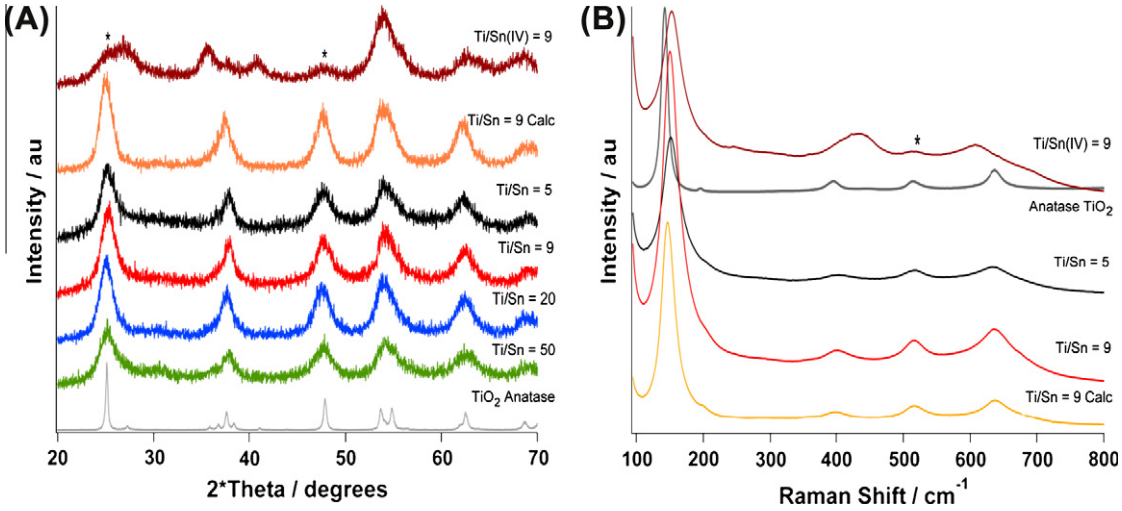

Fig. 1. XRD patterns (A) and Raman spectra (B) of Sn-doped TiO_2 photocatalysts. The corresponding data of commercial TiO_2 anatase are presented for reference. *Indicates the presence of anatase crystal peaks or Raman bands observed for Sn^{4+} TiO_2 photocatalyst which is predominantly rutile.

Table 2
Properties of Sn–TiO_2 photocatalysts synthesized from chloride precursors.

Ti/Sn	(200) position (2θ degrees)	Particle size[1] (nm)	Raman E_g position (cm^{-1})	Raman E_g FWHM (cm^{-1})	Band gap (eV)	Surface area[2] ($m^2\ g^{-1}$)	Mesopore volume[3] ($cm^3\ g^{-1}$)	Pore size, (nm)
5	47.54	5.1	152	27	2.47	225	0.147	2.7
9	47.58	4.9	150.5	25.7	2.61	226[4]	0.179[4]	3.5[4]
20	47.80	4.9	150	24.9	2.79	225	0.213	4
50	47.82	9	–	–	2.86	286	0.448	Bi-modal
9-Sn^{4+}	[a]	[a]	[a]	[a]	3.15	215[5]	[b]	[b]
9-Calc	47.60	6.2	147	21.9	3.23	162	0.164	4
Anatase	47.87	32	142.5	11.4	3.18	–	–	–

([1]) Calculated using the FWHM of the (200) reflection and determined using the Scherrer equation, the standard deviation is 3 $m^2\ g^{-1}$ ([2]) and 0.005 $cm^3\ g^{-1}$ ([3]), for the same tin loading but synthesized from bromide precursors, the values are 238 $m^2\ g^{-1}$, 0.163 $cm^3\ g^{-1}$, 2.6 nm ([4]), and 211 $m^2\ g^{-1}$ ([5]).
[a] The formation of a rutile and not a anatase polymorph of TiO_2 precludes this analysis.
[b] For 9-Sn^{4+} material, the shape of the adsorption isotherm precludes reliable determination of these quantities.

lower loadings while the rutile phase develops at higher loadings. We have not varied the tin content in this case as the band gap was always in the UV region. No additional phases, namely SnO, SnO_2, or Sn_3O_4, were observed in the XRD patterns of all Sn-doped titania products.

The Raman spectra show no evidence of the presence of tin oxides, as also observed in the XRD patterns. For the Sn^{4+}-doped TiO_2, the material showed Raman emission bands of the rutile (predominant) and anatase phases. For the tin-doped anatase samples obtained using $SnCl_2$, six bands (E_g, B_{1g}, A_{1g}) consistent with the $I4_1/amd$ (141) space group of anatase TiO_2 are observed although they are blue-shifted and broad relative to the commercial anatase standard (Fig. 1b). These data are presented in Table 2 (see also Figs. S10 and S11 in the supporting information section). The blue-shift has been observed for Sn^{4+}-doped TiO_2 and for titania nanoparticles and can be explained, in part, using the phonon confinement model [35,36]. As within these small crystallites (Table 2) complete wave vectors cannot be generated, there are off-center phonons contributing to the Raman bands, and a broadening of the phonon momentum and a subsequent blue-shift in the Raman bands is observed. This blue-shift in Raman bands is not linear (see Fig. S10), suggesting that apart from phonon confinement, oxygen vacancies contribute to the blue-shifts and peak broadening [36]. The *calcined* Ti/Sn = 9 sample is a clear outlier (Table 2), and the lower FWHM of the E_g Raman band and less pronounced Raman blue-shift is probably due to a lower concentration of vacancies because of the calcination step.

Nitrogen adsorption measurements show that all the tin-doped titania catalysts are mesoporous and have around five times higher surface areas than the commercial P25 photocatalyst (Table 2). The samples with 5, 9, and 20 Ti/Sn ratios have increasingly larger mesopore volumes as indicated by shape of the hysteresis loop starting at $P/P_0 \sim 0.4$. The isotherm of the sample synthesized with Ti/Sn ratio of 50 is a combination of Type I and Type IV isotherms (see Fig. 2) [37,38]. The steep increase in the volume adsorbed in the low pressure region ($P/P_0 < 0.05$) is indicative of micropores (Type I) [38]. There is also a complex hysteresis loop between P/P_0 of 0.5 and 1 indicating the presence of mesopores (Type IV) with a broad pore size distribution (Fig. 2b). The lack of a limiting adsorption at high P/P_0 regions is a characteristic of macropores. Altogether, the pore size and pore volume decrease with increasing tin content implying that the packing of the Sn–TiO_2 particles becomes denser with increasing tin incorporation (Table 2).

The particles observed by SEM do not have any particular morphology but are rather an agglomeration of poly-disperse nanoparticles (Fig. S16). The measured tin-to-titanium ratios are close to the synthesis values, indicating no loss of tin or titanium during the synthesis or washing procedures (Table 3). Notice, in the EDAX data, that there is chlorine in the solid products from the $SnCl_x$ precursors. Previous reports [12,34,39] on tin-doped TiO_2 have also indicated the presence of halogens from the halide precursors generally employed. The Cl/(Sn + Ti) contents increase with tin loadings from 0.004 (Ti/Sn = 50) to 0.079 (Ti/Sn = 5). Halogen incorporation into the solid product is possibly a consequence of

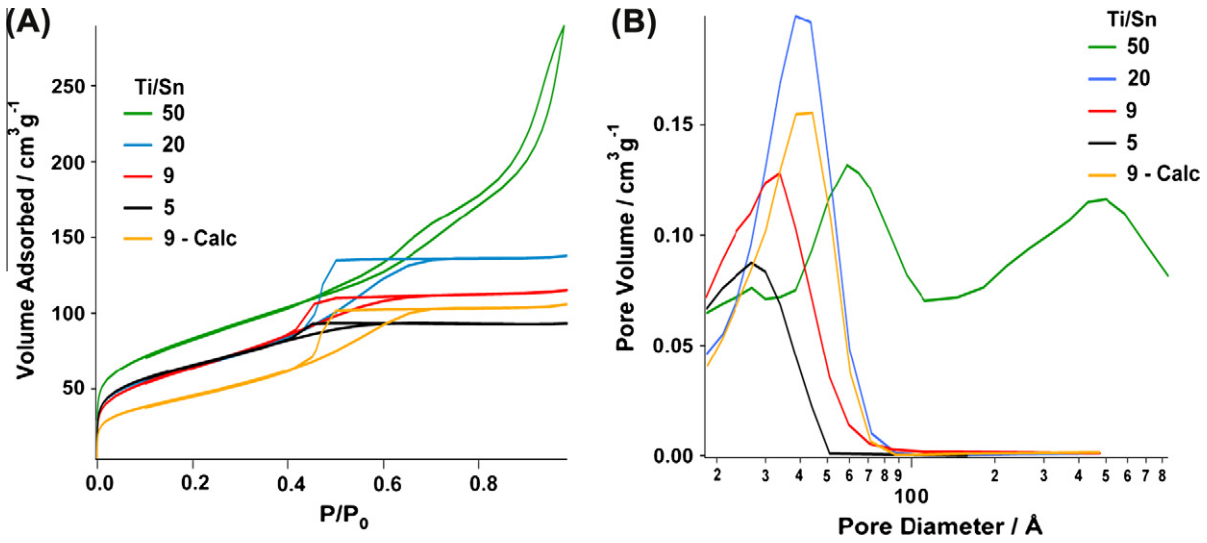

Fig. 2. N_2 adsorption–desorption isotherms (A) and pore size distributions (B) of the Sn–TiO_2 photocatalysts.

Table 3
Surface and bulk compositions obtained from SEM-EDAX and XPS for samples synthesized using tin chloride precursors.

Ti/Sn	Bulk composition		Surface composition					
	Ti/Sn	Cl/(Sn + Ti)	Ti/Sn	Cl/(Sn + Ti)	Sn^{2+}/Sn^{4+}	OH/(LO + OH)	Ti edge (eV)	Lattice O edge (eV)
SnO_2	–	–	–	–	–	–	–	530.8
5	4.85	0.08	1.65	0.17	1.28	0.22	458.5	530.0
9	9.1	0.04	1.87	0.13	1.65	0.13	458.6	529.9
20	19.1	0.03	3.81	0.12	2.11	0.08	458.4	529.9
50	56.9	0.004	–	–	–	–	–	–
9-Sn^{4+}	9.35	0.07	4.14	0.13	0	0.11	458.7	530.2
9-Calc	9.06	0.03	3.41	0.09	0	0.05	458.5	529.9
Anatase	–	–	–	–	–	–	458.4	529.8

tin incorporation, thereby causing the anion environment to decrease its total charge. This can be brought about either by forming defects (oxygen vacancies) or by bringing an anion with a lower oxidation state, in this case is the halide (Table 3) [34].

When the source of tin is $SnCl_2$, all the tin-doped catalysts showed absorbance in the visible region with the band gaps decreasing with increasing tin content (Tables 2 and 3). There is no consensus into the effects of tin doping on the electronic structure of titania (Table 1) but Sn^{2+}-containing oxides like $Sn_2Ta_2O_7$ (3.0 eV) and $Sn_2Nb_2O_7$ (2.3 eV) have smaller band gaps compared with $Ca_2Ta_2O_7$ (4.4 eV). These reductions in band gap are attributed to a change in the position of the valence band because of the introduction of Sn 5s orbitals [10,11,40]. Hybridizations in the valence band due to s orbitals have been observed with $Bi^{3+}(6s^2)$ [8,9] and thus the reduction in the band gaps of the samples prepared here is likely associated with the presence of Sn^{2+} cations in the structure (Fig. 3A). Note that most of cation-doped titania investigated in the past give rise to mid-gap states (which act as detrimental electron traps) [7] but the materials described here are distinct in that they are modified at the valence band (VB) level due to the presence of a hybridized (Sn^{2+} 5s–O 2p) and thus a dispersed VB leading to a better mobility of holes [8].

Chlorine-doped TiO_2 has lower band gaps than pure TiO_2 (from 3.17 eV for P25 to 2.99 for Cl–TiO_2) [41]. Chlorine is present in the samples synthesized either with $SnCl_2$ or with $SnCl_4$ precursor (Table 3); still the latter sample does not exhibit an absorption spectrum in the visible region (Fig. 3A). Thus, the presence of the halide is not the sole reason for the reduction in the band gaps of the Sn(II)-doped TiO_2 materials. This is illustrated in the calcined Ti/Sn = 9 sample which also has Cl (as determined from EDAX and XPS, Table 3), but where the Sn^{2+} cations are oxidized to Sn^{4+} upon calcination at 300 °C [19,24,40]. The oxidation of the sample increases the band gap to 3.23 eV, and thus, chlorine by itself does not play a role in the band gap reduction [42] of TiO_2. To clarify the role of Cl, the precursor was replaced with $SnBr_2$ keeping the Ti/Sn ratio of 9. The resultant product is again anatase with a similar Ti/Sn ratio (from EDAX). Although the absorption spectrum is red-shifted to the visible region, it is not identical to that obtained using $SnCl_2$ (Fig. 3b) indicating that the halogen ions in the precursor do influence the electronic properties of tin-doped titania.

Other reports have suggested the formation of a new level below the conduction band from the isomorphous substitution of Sn^{4+} for Ti^{4+} in rutile TiO_2 [20]. We observed no reduction in the band gap for the rutile Sn^{4+}-doped samples in agreement with other theoretical and experimental results [14,21]. Irrespective of the precursor ($SnCl_4$ or $SnBr_4$) and the presence of the halide, rutile tin-doped TiO_2 shows no reduction in the band gap. The results from diffuse reflectance measurements agree well with the observations by Ghosh et al. [24] They have shown using Mossbauer spectroscopy that the tin in $SnCl_2$-synthesized samples (with Ti/Sn = 9) is a combination of tin in both Sn^{2+} and Sn^{4+}, the former in two different sites. When this sample was calcined in air, the Sn^{2+} is oxidized to Sn^{4+} leading to an increase in the band gap. However, although the reduction in the band gap is mostly from the presence of Sn^{2+}, the effect of halogen ions should not be neglected. Further experimental investigations are needed to clarify the extent of interaction between tin and co-dopants (halides in this case) in the solid products.

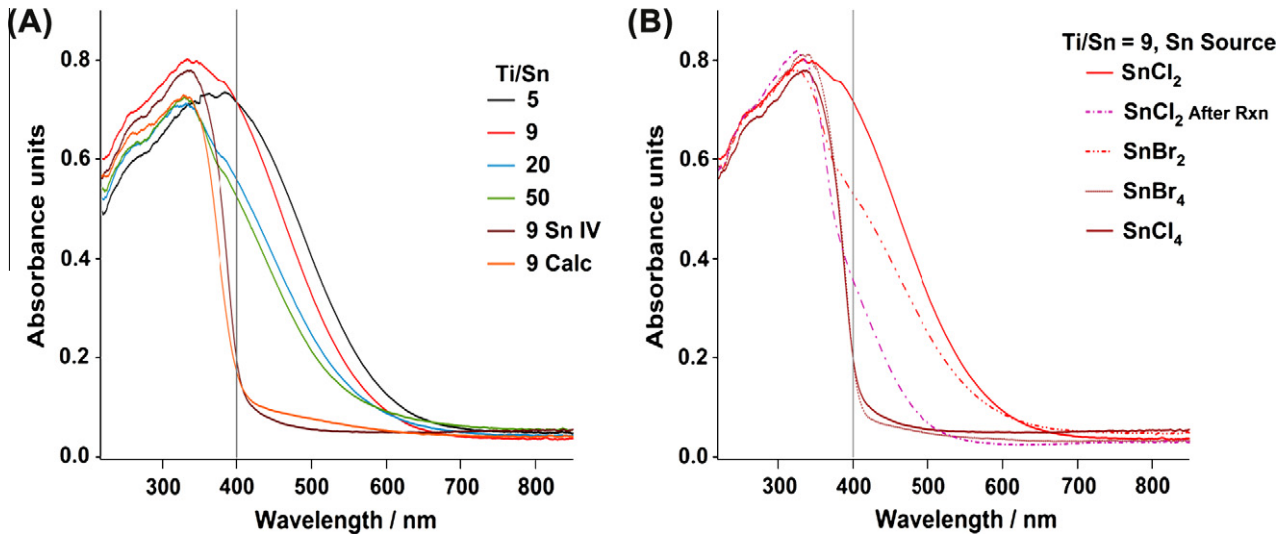

Fig. 3. UV–vis diffuse reflectance spectra of Sn–TiO_2 photocatalysts synthesized from chloride precursors (A), and the differences in the optical (visible region) properties when synthesized from bromide precursors (B).

3.2. Photocatalytic activity

One pathway of photocatalytic degradation is via indirect oxidation by hydroxyl radicals ($OH^{\bullet}$). Our photocatalysts are expected to degrade organic molecules using visible light from the generation of these species (Fig. 4). Their concentration can be followed by the reaction between terephthalic acid and the $OH^{\bullet}$ species to form 2-hydroxy terephthalic acid, a molecule with a fluorescence band at 425 nm [33]. When the catalyst is introduced into the solution, there is a linear increase in the fluorescence intensity at 425 nm confirming the formation of hydroxyl radicals using visible light (Fig. 4). Very few hydroxyl radicals are produced in visible light with no catalyst. Photodegradation of RhB dye was used to test for the photocatalytic activity. As the molar extinction coefficients of the various RhB degradation species are very similar, [43,44], the concentration changes of the dye can be monitored by observing changes in the maximum absorbance of the chromophore with time. The degradation rate of RhB is noticeably faster than that observed with the reference P25 in 4 h of illumination using visible light when the Ti/Sn ratio is 20 and 50. However, it is lower than P25 TiO_2 when the Ti/Sn ratio is 5 and 9 (Fig. 6c). It can be shown that the mechanism of degradation is via de-ethylation for the first two samples (Ti/Sn of 20 and 50), whereas it is via direct ring oxidation in the last two (Ti/Sn is 9 and 5, see Fig. 6d). Distinct mechanisms of dye degradation has been attributed to differences in the extent and modes of dye adsorption [45–47], catalyst's surface charge [48], photogenerated species involved [47,49], and catalyst defects [46]. The catalyst (Ti/Sn = 20) with the highest activity for RhB degradation also shows the highest dark adsorption (Fig. 6c), and an enhanced adsorption of dyes on the catalyst surface has been ascribed to specifically cause N-de-ethylation on TiO_2-based materials [45,46] as this mechanism is mostly a surface process [47]. In fact, it is the only Sn-doped TiO_2 sample to completely decompose the dye's chromophore using visible light (see Section 4.1.1), while all the Sn(II)-doped TiO_2 samples were able to completely decompose the dye when the full spectrum of the light source is used. The photocatalytic activity in visible light (for degradation of RhB in 4 h of illumination) is ranked accordingly as (Ti/Sn=) 20 > 50 > P25 > 5 > 9.

Addition of H_2O_2 can increase the rate of degradation of organic compounds by increasing the concentration of oxidizing $OH^{\bullet}$ [50,51]. To test this possibility, the less active materials were analyzed for dye degradation after the addition of 1 ml of 30 wt.% H_2O_2. Complete degradation of the dye is achieved in visible light in all cases within the illumination times investigated. In the presence of H_2O_2, the rates are slower compared with P25 TiO_2 (also with H_2O_2) when the Ti/Sn content is 5 and 9 but faster when the ratio is 50 (Fig. 6e). Note that with the addition of H_2O_2, no dye de-ethylation was observed in visible light.

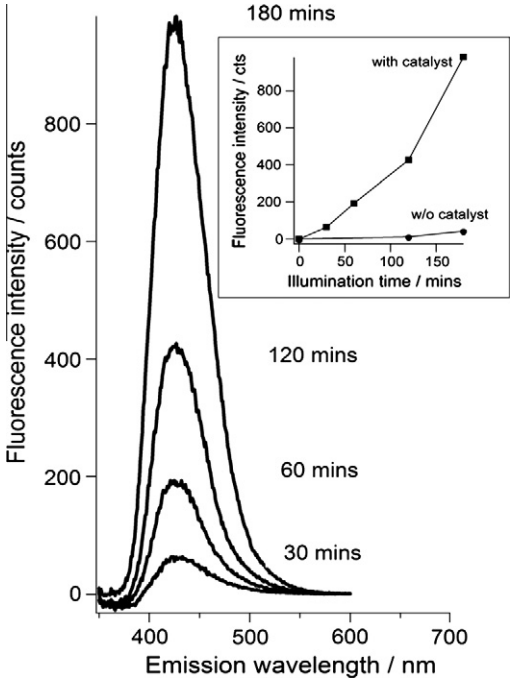

Fig. 4. Formation of $OH^{\cdot}$ radicals generated under visible light from the formation of hydroxyl terephthalic acid, the inset shows the temporal profile of the increase in intensity of its PL band with time, catalyst used Ti/Sn = 9 ($SnCl_2$ precursor).

4. Discussion

4.1. Surface structure of TiO_2 upon tin doping

Sn^{2+} (r = 112 pm) and Sn^{4+} (r = 69 pm) ions are larger than Ti^{4+} (r = 60.5 pm), and the incorporation of these ions into the crystal

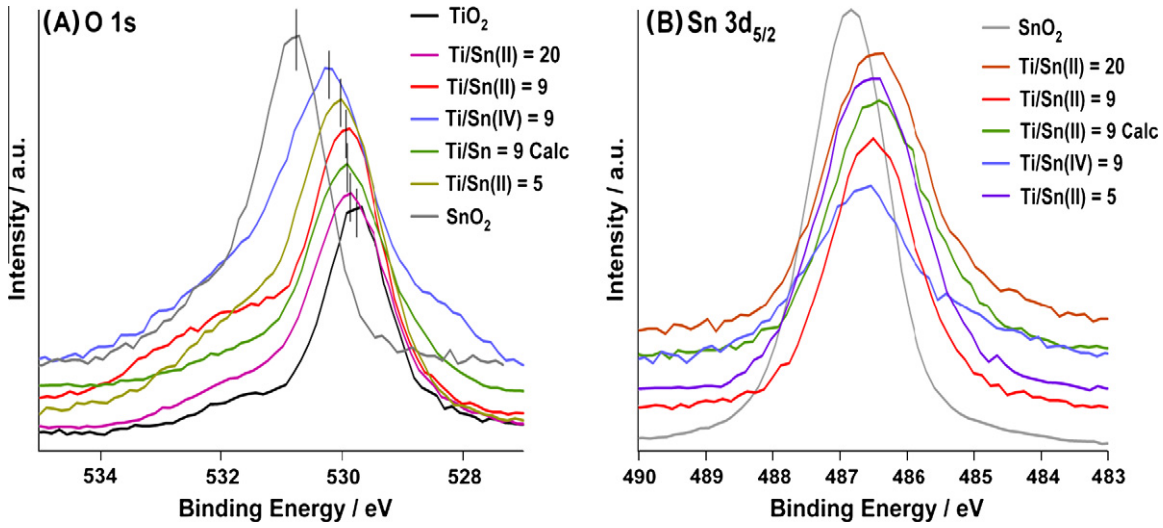

Fig. 5. O1s (A) and Sn $3d_{5/2}$ (B) XPS spectra of the various Sn–TiO_2 samples.

should lead to an increase in the unit cell volume. In our case, it is not possible to reach a definitive conclusion regarding unit cell volume changes because of the broad diffraction peaks, but any changes in unit cell volume are small. Similar observations have been made before [12,18] studying Sn^{4+}–TiO_2 systems although small shifts to lower diffraction angles were observed for the (200) peak at ~47.5° 2θ (Table 2). It is known that anatase is a more flexible polymorph of TiO_2 with a larger c/a ratio than rutile [24], and thus, this could be the reason why the synthesis using the larger Sn^{2+} cations forms the anatase crystal structure. SnO_2 and TiO_2 can crystallize in the rutile crystal form (Ti^{4+} and Sn^{4+} have similar ionic radii), and it is reasonable that synthesis using SnX_4 precursors leads to the nucleation of rutile crystals [39].

The presence of amorphous overlayers or small quantities of SnO and SnO_2 in the product can be ruled out as no bands were observed in the UV–vis spectra [42] or photoluminescence measurements associated with these oxides. The thickness of the SnO overlayer if possible with assumptions [52] could be about 2 Å for the Ti/Sn = 5 sample and about 0.2 Å for the Ti/Sn = 50 material. So, it could be about a monolayer thick for the high tin loading and just a fraction for the low loading. Both PL and UV–vis techniques are much more sensitive to the presence of additional phases than XRD [53]. For example, Jianhui et al. [53] have observed an additional low intense UV–vis band at 270 nm, which they have attributed to ZnO apart from their desired band at 220 nm for Zn_2GeO_4 (4.5 eV). This additional ZnO (3.2 eV) phase was not detected in their XRD patterns. PL measurements show that oxygen vacancies and defects that lead to electron–hole recombination in the case of commercial anatase TiO_2 are still the origin of PL bands for Sn^{x+}–TiO_2 catalysts as no additional bands were detected in the doped samples (Fig. S14) [54]. Alternatively, it could be that the dopants are dispersed on the surface of titania, i.e., the cation sites on the surface are taken by Sn^{2+}. It is likely that as the anatase crystals grow in solution, the bigger tin cations coordinate with O forming Sn^{x+}–O–Ti bonds on the growing particle. If these two phenomena occur in tandem, apart from the expected Ti/Sn in the bulk from EDAX, the surface Sn content would be higher than the bulk ratios, and since Sn^{2+} is a larger cation than Sn^{4+}, a higher surface ratio of Sn^{2+}/Sn^{4+} is also expected. A similar explanation has been offered before for Y^{3+}- (r = 90 pm) and Rb^+ (r = 152 pm)-co-doped TiO_2 [55] and Ag^+ (r = 115 pm)-doped TiO_2 [56].

The surface composition (Table 3) shows that the Ti/Sn surface ratios are much lower than the bulk. The surface is indeed composed of more tin than titanium and the former mostly as Sn(II), as it is the biggest cation. Although the surface tin content is higher, the EDAX data and XRD peak shifts suggest the presence of some tin in the bulk [57]. These experiments do not support the possibility of all the tin present as amorphous surface overlayers of SnO or SnO_2 [15,58,59]. In particular, we do not observe a new Raman band at 560 cm^{-1}, observed by Dieguez et al. [59] for SnO_2 particles with a SnO_x shell, and this band was attributed to a disordered SnO_x surface species, which is only 1.1 nm thick. The surface Sn contents for the calcined anatase and rutile tin-doped titania materials are lower than the corresponding Sn^{2+}-doped anatase TiO_2 solid products (Table 3) probably because Sn(IV) is less unstable than Sn(II) in the bulk because of a better match in the ionic radii for Sn^{4+} (r = 69 pm) with Ti^{4+} (r = 60.5 pm), note that there is a coalescence of particles with calcination leading to a reduction in the surface area.

The XPS measurements suggest the formation of Sn–O–Ti bonds as the Ti $2p_{3/2}$ (Fig. S12) and lattice oxygen O 1s (Fig. 5A) binding energies (BE) increase slightly with increasing Sn content. The product's Ti edge is shifted to higher BE (by ~0.2 eV) relative to the Ti $2p_{3/2}$ peak position of commercial anatase TiO_2. The O 1s peak position is in between the BE observed for anatase TiO_2 and SnO_2 standards (Table 3). This shift is expected because of a shift in electron density from a lower electronegative Ti (1.54, Pauling scale) to a more electronegative Sn (1.96) atom. Ghosh et al. [24] using Mossbauer spectroscopy, have proved that the presence of tin in $SnCl_2$-synthesized samples is a combination of both Sn^{2+} and Sn^{4+}, the former in two different sites. When this sample was calcined in air, the Sn^{2+} is oxidized to Sn^{4+}. This information was utilized for XPS peak fitting, and thus, the Sn $3d_{5/2}$ lines for materials synthesized using $SnCl_2$ precursor were fitted to 2 peaks corresponding to Sn^{2+} and Sn^{4+}. No clear trend in the peak shifts of Sn $3d_{5/2}$ was observed with respect to the tin loading, although the binding energies are clearly below that of SnO_2 (Fig. 5B) [60]. The smaller decrease in the XPS binding energy of Ti $2p_{3/2}$ has been earlier observed for Sn^{4+}–TiO_2 samples synthesized by Li and Zeng [34]. Similar to the shifts observed here, they have observed only a small positive shift 0.2 eV for Ti $2p_{3/2}$ relative to TiO_2 but a prominent negative shift of 0.5 eV for Sn $3d_{5/2}$ relative to SnO_2. XPS measurements, then, indicate a higher concentration of tin on the surface than in the bulk, the former mostly as Sn^{2+}. It is known that the shift in binding energies of the Sn 3d level with respect to its oxidation state is minimal (0.5–0.7 eV), as observed for Sn(II)–Sn(IV) [60,61] and Pb(II)–Pb(IV) [62], although lower binding energies of the peak attributed to Sn^{2+} are generally observed relative

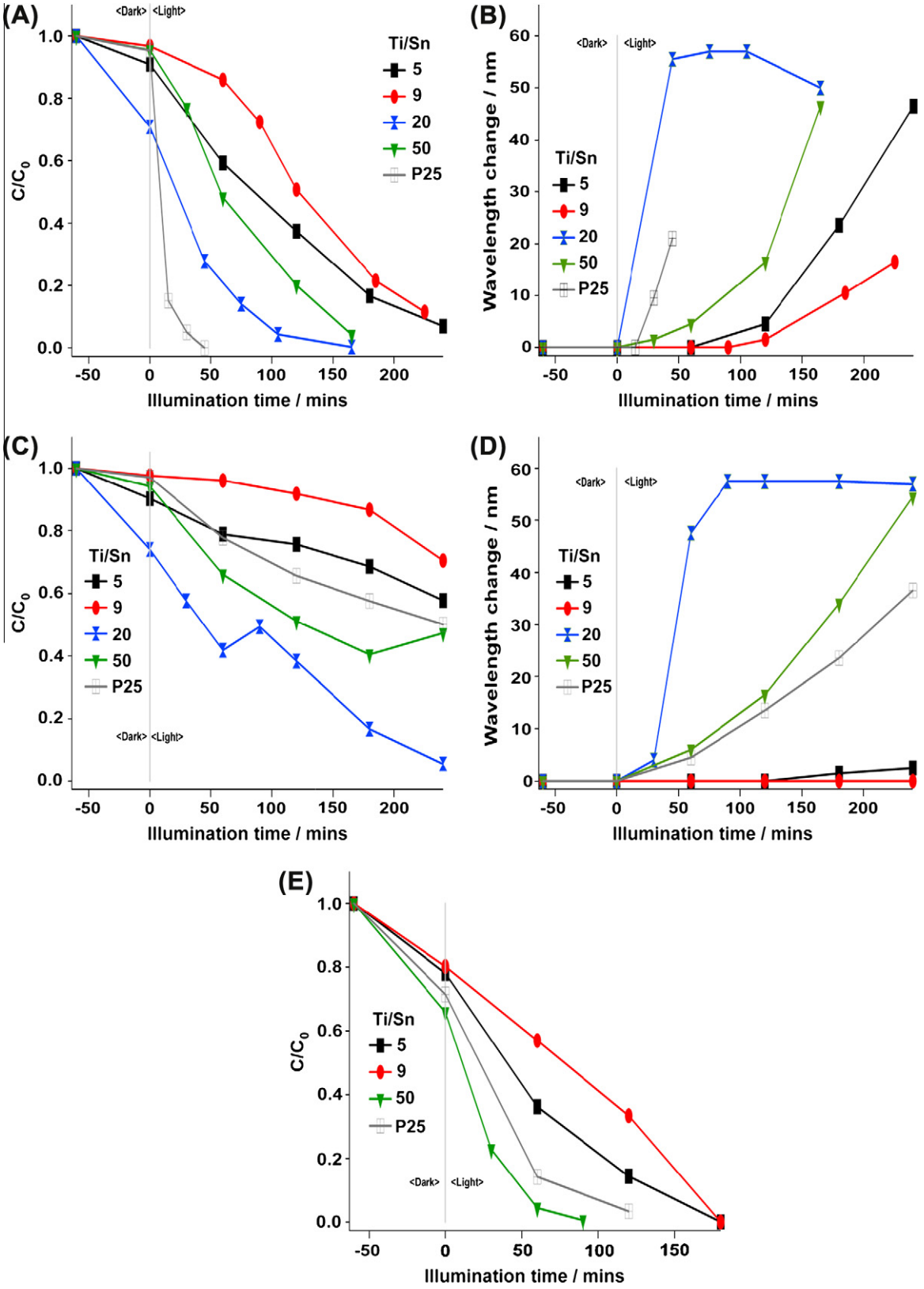

Fig. 6. The temporal profile of RhB decomposition and the change in wavelength of RhB with illumination time, respectively, in UV + visible (A and B) and visible (C and D) light with various Sn–TiO_2 catalysts ($SnCl_2$ precursor). Also presented are the conversions achieved using visible light with the addition of H_2O_2 (E), in this case, no N-de-ethylation of the dye was observed. See supporting information for control experiments.

to that of Sn^{4+}. This lack of prominent binding energy shifts for different oxidation states of tin is commonly attributed to Madelung effects [62]. Harunsani et al. [15] have reported oscillating changes in the Sn 3d line with increasing Sn content although they have also observed a linear increase in the BE of Ti $2p_{3/2}$ and O 1s peaks. Their samples are similar to ours and are composed of Sn^{2+} and

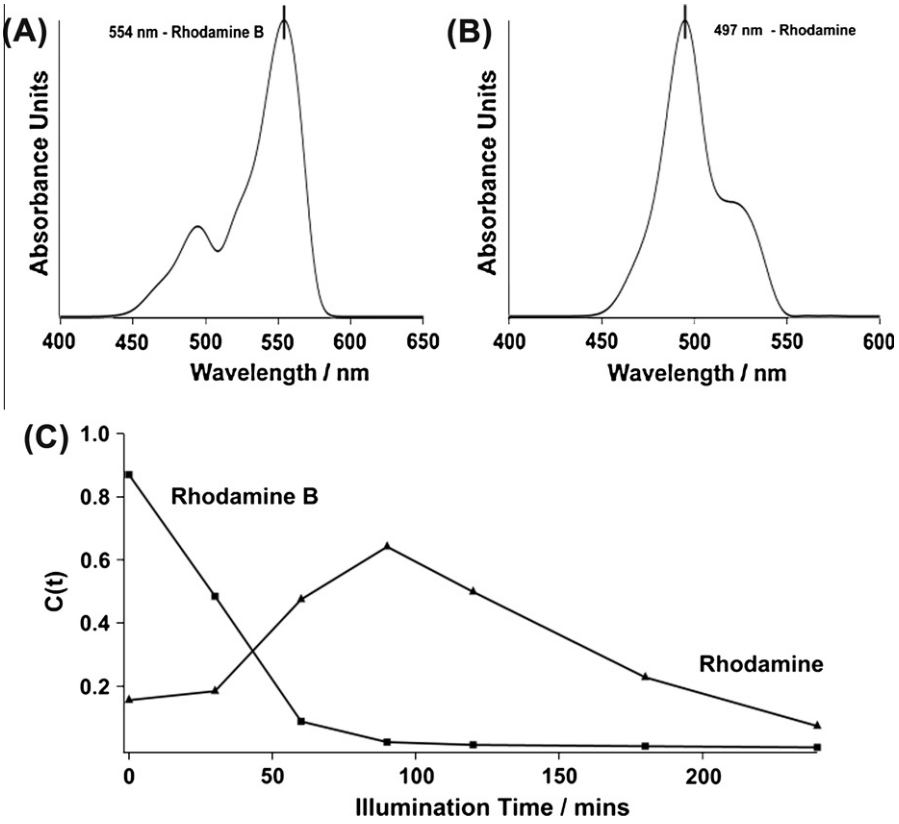

Fig. 7. The two dye decomposition species from chemometric analysis, RhB (λ = 554 nm) and Rh (λ = 497 nm), are presented in Figures B and C with Figure D representing the concentration changes (in absorbance units) with illumination time when using visible light. Ti/Sn = 20 ($SnCl_2$) catalyst.

Sn^{4+} surface species. XPS measurements indicate an interaction between the two cations via the oxygen anions with the formation of Sn–O–Ti linkages consistent with the shifts in the BE observed, but there is no evidence of the tin existing as SnO/SnO_2 layers on the surface of the particles [57]. Further experiments are required to determine firmly the oxidation state and location of tin in the titania framework.

The introduction of lower valent Sn^{2+} cations is bound to cause charge imbalances and oxygen deficiencies that are compensated in part by hydroxyl groups (Table 2), and even the introduction of Cl^- through ligand exchange will affect the surface hydroxyl groups when compared with undoped TiO_2 [63]. IR spectra (Fig. 9) were measured after heating the samples in vacuum at ~200 °C for 2 h to remove adsorbed surface water [63]. Anatase TiO_2 has 3 bands: 3719 (strong), 3670 (medium), and 3642 cm^{-1} (weak) as observed in Fig. 9. Bands above 3680 cm^{-1} for anatase are attributed to linear Ti–OH species, whereas those at lower frequencies can be ascribed to bridged hydroxyl species [63,64]. Upon the introduction of tin, the isolated hydroxyl species at 3719 cm^{-1} decreases in intensity, the 3670 cm^{-1} Ti–OH–Ti band disappears, and the previously low intensity band at 3642 cm^{-1} is now the most prominent. Thus, the introduction of Cl and Sn affects both types of hydroxyl species. The presence of an intense H_2O band between 3550 and 2500 cm^{-1} (not shown) even after heat treatment in vacuum is likely due to a strong binding sites between the adsorbed water molecules and the surface cation sites, thereby decreasing their desorption compared with anatase.

4.2. Photocatalytic activities with Sn–TiO_2 photocatalysts

Although P25 TiO_2 has a band gap of 3.2 eV, it still shows 50% conversion of RhB dye under visible light after 4 h of illumination. The dye degradation in this case proceeds due to N-de-ethylation as shown by the changes in the wavelength corresponding to a decrease in the absorbance (Fig. 6). Since P25 shows no absorption in visible light (>420 nm), this conversion is via photosensitization where the dye absorbs light and then passes an excited electron to the conduction band of P25 TiO_2 where the active species are generated [51]. This process occurs on TiO_2 because of an intimate contact between the semiconductor particles and the dye. The degradation profile for P25 TiO_2 in visible light is consistent with those reported for CdS [43] (λ > 540 nm) and TiO_2 [47] (λ > 420 nm) in visible light, and we did not observe any ring destruction [47].

For the Sn(II)-doped TiO_2 samples with low Sn contents (Ti/Sn = 20 and 50), the reaction proceeds via N-de-ethylation in visible light, as was the case with P25, but with a faster rate (Fig. 6c), and for the former sample, chromophore ring breaking step was observed. The sample with the highest rate of decomposition (Ti/Sn = 20) also had the highest dark adsorption of the dye (Fig. 6c). N-de-ethylation occurs on the surface of the photocatalyst whereas ring breaking occurs in the aqueous bulk phase [47], thus a higher rate of de-ethylation can be attributed to an enhanced adsorption of the dye on the Ti/Sn = 20 catalyst as previously noted for TiO_2 systems [45,46]. The reaction rate constants (Figs. S1–S3) if obtained assuming a first-order process do not capture mechanistic differences between the N-de-ethylation and chromophore decomposition steps. To overcome this problem, chemometric tools were utilized to analyze the N-de-ethylation decomposition profile when using this catalyst. The two species isolated during the reaction from the multivariate component analysis were assigned to tetraethylated rhodamine (RhB with λ = 554 nm) and the completely de-ethylated rhodamine (with λ = 497 nm) [43] and are consistent with the experimentally observed products (Figs. 6, S15 and Table S1). The temporal profile obtained from the chemometric analyses indicates that as RhB is deethylated in the first 90 min (Curve I, Fig. 7c), intermediates are simultaneously

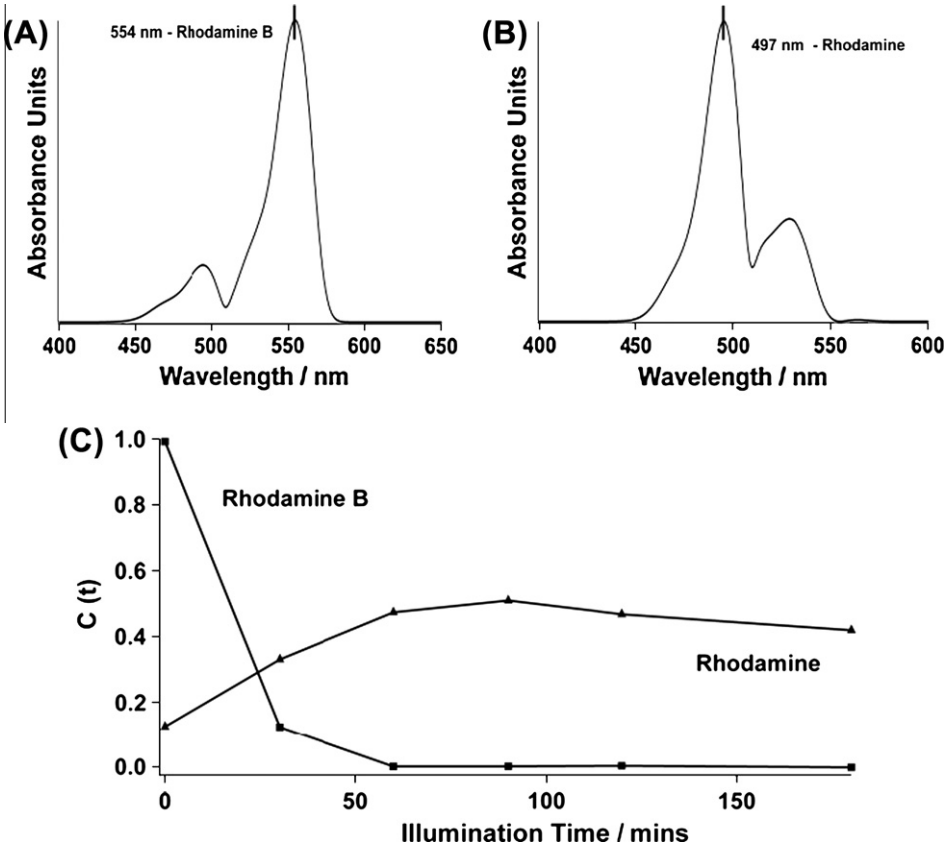

Fig. 8. The chemometric analysis of temporal profile of RhB decomposition in visible light with Ti/Sn = 9 ($SnBr_2$); the 2 species from chemometric analysis, RhB (λ = 554 nm) and Rh (λ = 497 nm), are presented in figures A and B, figure C representing the concentration (in absorbance units) changes with illumination time of the two 'pure' species.

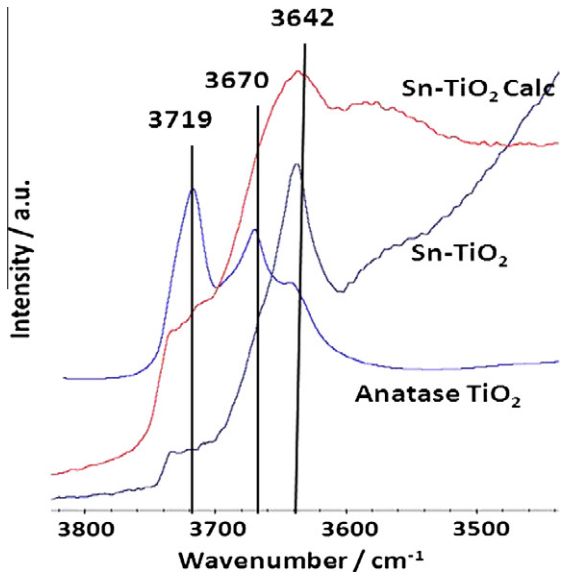

Fig. 9. Infra red spectra of Ti/Sn = 9 photocatalysts ($SnCl_2$ synthesized) and commercial anatase TiO_2 for comparison.

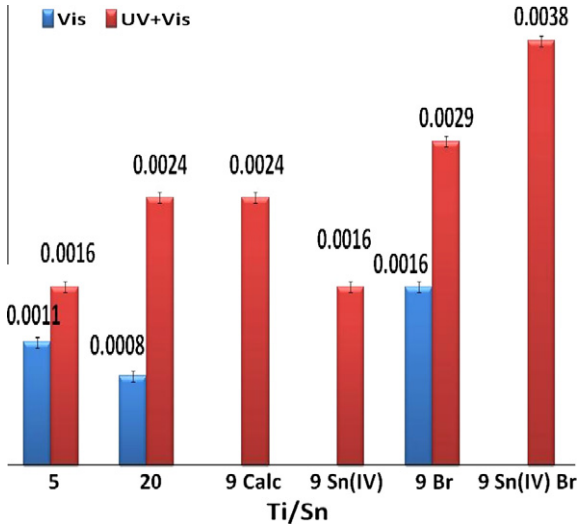

Fig. 10. Effective first-order cresol degradation rate constants when using different Sn–TiO_2 photocatalysts in UV + visible and visible light alone (see supporting information for control experiments).

generated (Curve II) whose chromophores are subsequently broken down at longer illumination times (>90 min) as with previous observations of RhB decomposition over visible-light-active $NaBiO_3$ [65].

This is an innovative application of chemometrics to isolate dye degradation intermediates and to elucidate the decomposition mechanism compared with the profile shown in Fig. 6c. The application of chemometrics is also useful to understand a similar decomposition curve over Ti/Sn = 9 ($SnBr_2$) catalyst, wherein there is an apparent concentration *increase* due to an increase in the concentration of the intermediates from 30 to 90 min of illumination (this catalyst shows around 20% dye adsorption in the dark). Fig. 8, obtained from the chemometric analysis, better represents

the temporal profile that is shown in Fig. 11a. These results are clearly different to the measurements using Ti/Sn ratio of 5 and 9 ($SnCl_2$ precursor), where no such N-de-ethylation of the dye molecules was observed (Fig. 6).

Sn–TiO_2 catalysts then clearly show visible light activity toward degradation of RhB dye molecules albeit with different degradation mechanisms depending on the tin content. The catalyst after the photocatalysis reaction exhibited a shift to higher energy in its absorption spectrum, though still showing absorbance in the visible (Fig. 4b). This blue-shift is most likely from the oxidation of a fraction of Sn^{2+} species to Sn^{4+} by photogenerated holes during photocatalysis much like what is observed when layered titanates and niobates ion exchanged with Sn^{2+} are used as photocatalysts [10].

Although direct photolytic degradation of dyes is slow (Fig. S4), the decomposition mechanism is complicated by the presence of a number of degradation channels. For the Sn–TiO_2 catalysts, measurements were conducted to show that the samples are active in visible light by also testing for the aqueous phase degradation of o-cresol. The samples investigated for visible light activity have Ti/Sn = 20 and 5 and show higher and lower conversions for dye degradation than P25 TiO_2, respectively, in 4 h of visible light illumination. However, for the oxidation of cresol (Fig. 10), the Ti/Sn = 5 sample shows higher visible light reactivity in contrast to RhB degradation where the Ti/Sn = 20 is the most active. This difference in the order of visible light activity is probably due to different photocatalytic decomposition mechanisms of the two compounds; N-de-ethylation of RhB dye on Ti/Sn = 20 proceeds due to the formation $OH^{\bullet}_{surf}$ at the conduction band, and this is associated with the dyes' strong adsorption on the catalyst surface (Fig. 6c), whereas cresol degradation is via direct hole oxidation [46,66] and the mobility of holes increases in the now dispersed valence band and has been noted for $BiVO_4$ and $CaBi_2O_4$ (in these cases due to introduction of Bi 6s) [8,9]. The Ti/Sn = 5 catalyst was also found active for visible light degradation of phenol and chlorophenol (see SI). Because of the electron withdrawing nature of the substituent, the photocatalytic rates are in the order of chlorophenol > cresol > phenol. Note that the visible light activities observable for cresol degradation with these novel materials are in contrast to that noticed with P25 and anatase TiO_2, wherein the degradation of cresol proceeds via the formation of quinone-based intermediates (the reactant solutions turn brown) [67] leading to an increase in the UV–vis band at 272 nm indicating an apparent concentration increase [66] and in agreement with the multistep degradation of phenol detailed by Sobczynski et al. [68] These intermediate species were not decomposed even after exposure to visible light for 4 h when using P25 and anatase TiO_2 as only a limited decrease in the intensity of the associated UV–vis band was observed [66]. Therefore, the degradation of phenolic compounds proceeds efficiently over Sn–TiO_2 materials unlike with P25 and anatase TiO_2.

4.3. Effect of H_2O_2 on photocatalytic activity

Organic molecules can be degraded in aqueous phase via attack by hydroxyl radicals generated either from the dissociation of H_2O_2 (at the conduction band) or from the reaction between the holes, H_2O, and hydroxyl anions (at the valence band). A factor that limits photocatalytic activity is recombination of electron–hole pairs, and thus if the rate of recombination between h^+ and e^- is decreased while the oxidizing hydroxyl radical concentration is increased, the reaction rates are expected to increase. This can be achieved in practice by the addition of H_2O_2 because of its role as an electron scavenger (reaction 4) [50,51]:

$$H_2O_2 + e^- \rightarrow OH^- + OH^{\bullet} \quad (4)$$

As can be seen from Fig. 6e, the catalysts that did not show 100% degradation using visible light show now an enhanced rate in the presence of hydrogen peroxide. This rate increase is not from the photodissociation of H_2O_2 to $OH^{\bullet}$ as H_2O_2 does not absorb visible light and the control experiments (see SI) also show little reactivity when H_2O_2 is utilized with no catalyst in visible light. P25 TiO_2 also shows an increase in the activity in visible light, although it does not absorb visible light (3.2 eV). This phenomenon has been documented by Li et al. [69] and has been attributed to the formation of Ti^{4+}–OOH species, which extends the absorbance spectrum of TiO_2 into the visible region. Now, the dye decomposition mechanism on all the catalysts does not proceed via de-ethylation but via the chromophore ring breaking (as no hypsochromic shift was observed). This is ascribed to the formation of hydroxyl radicals in the bulk solution [47]. Although the addition of hydrogen peroxide increased the rates substantially, the overall trend for RhB decolorization still remains the same: catalysts with higher tin content (Ti/Sn = 5 and 9) are less active than the Ti/Sn = 50 catalyst. This

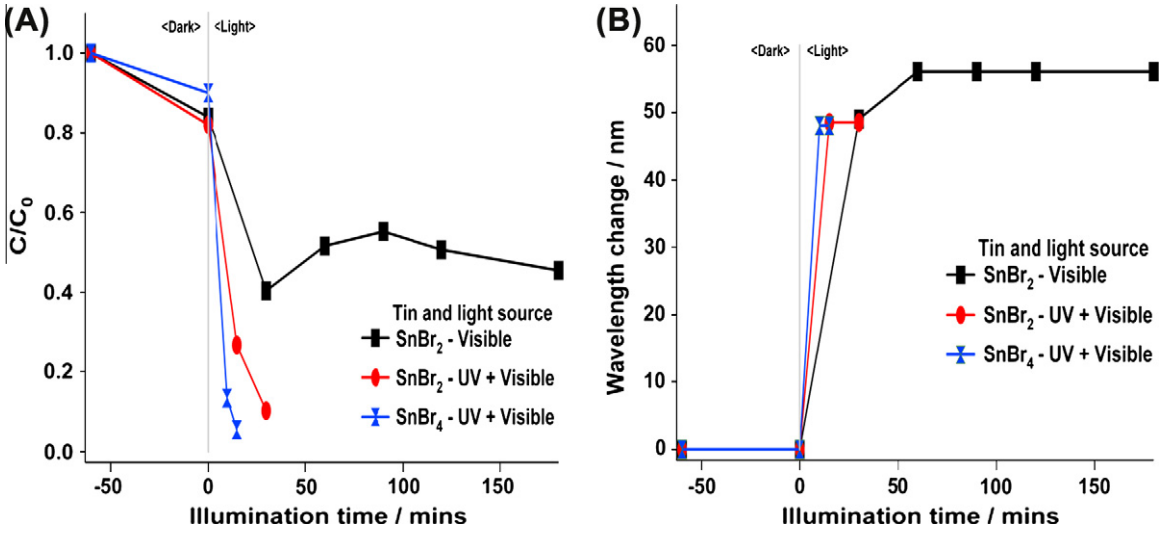

Fig. 11. The temporal profile of RhB decomposition (A) and the change in wavelength of RhB (B) with illumination time in UV + visible and visible light with various Sn–TiO_2 catalysts synthesized from $SnBr_x$ precursors.

sample shows higher activity compared with the P25 TiO_2 reference with H_2O_2, although with H_2O_2, all the tin-doped samples show enhanced activities compared with just P25 TiO_2 (Fig. 6e).

In contrast, upon addition of hydrogen peroxide for the photodegradation of cresol, the degradation rate actually decreased (refer to Fig. S6). This rate reduction is due to the formation of quinone-based intermediates from the reaction between OH· (from H_2O_2 addition) and cresol (Eq. (5)). These quinone compounds are detected in the UV–vis spectra of cresol, which now show an apparent concentration increase in the dark and during short illumination times as has been witnessed for oxidation of phenol with C_3N_4 photocatalysts [66,67].

$$OH^{\cdot}(H_2O_2) + \text{Cresol} \rightarrow \text{quinone-based intermediates} \quad (5)$$

4.4. Effect of precursor on activity

Investigations on the degradation of RhB and cresol using Sn-doped titania photocatalysts synthesized from bromide-based precursors demonstrated significant differences in degradation rate to chloride-based systems. The photocatalytic activity of Cl- and Br-derived catalysts is as follows: when using the full spectrum of the xenon lamp, the Br-derived samples show a pronounced increase in the degradation rates of RhB and cresol (observed for both the anatase and rutile forms, Figs. 10 and 11). In the presence of visible light alone, RhB degradation on the sample synthesized from $SnBr_2$ proceeds via N-de-ethylation and the chromophore break-up step is slow (Figs. 8 and 11), unlike the $SnCl_2$-synthesized sample with the same Ti/Sn = 9 which showed no formation of de-ethylated intermediates (Fig. 6c). This bromide-synthesized Sn^{2+}-doped product also exhibits degradation rates for cresol compared with the Cl samples (Fig. 10). Therefore, for Sn^{2+}–TiO_2 samples obtained using halide precursors, the optical and catalytic properties are unique to the sample and the halogen effects could be one of the reasons behind the variability exhibited by tin-doped titania photocatalysts in literature (Table 1).

5. Summary and conclusions

We provide evidence of photocatalytic activity of mesoporous tin(II)-doped titania materials synthesized by a reaction between tin precursors and titanium butoxide. When the precursor employed is $SnCl_2$, anatase products with band gap in the visible region were obtained due to electronic contributions from Sn^{2+} 5s orbitals. The presence of tin as surface overlayers of SnO and SnO_2 was ruled out. The overall Ti/Sn ratio was similar to the ratio in the synthesis gel, although the surface is composed of more tin (mostly as Sn^{2+}) than in the bulk as determined from XPS. These products are highly active for the degradation of organic molecules with the Ti/Sn = 20 and 5 photocatalysts being the most active for RhB and cresol degradation reactions, respectively. While the Sn-doped titania samples do generate oxidizing hydroxyl radical species in the presence of terephthalic acid, further work is needed to increase their photostability. The addition of hydrogen peroxide increased the rates of dye decomposition, whereas it has a negative effect for the decomposition of cresol. Interestingly, upon calcining the Sn^{2+}-doped catalysts, the resultant product – still the anatase polymorph – has no longer a band gap in the visible region due to the oxidation of Sn^{2+} to Sn^{4+}. When the precursor employed was changed to Sn(IV) halides, Sn^{4+}-doped rutile polymorph of titania was observed albeit with band gaps in the UV region (>3 eV). The catalyst's electronic properties and activities were found to depend on the co-dopant halide. These effects need to be clarified with more experiments and could explain the differences in reactivity and electronic properties observed in literature. Chemometric methods of analyses were applied to understand the de-ethylation mechanism of dye decomposition, and the calculated products and time profiles are consistent with the experimentally observed absorption spectra of the dye species.

Acknowledgments

The authors would like to acknowledge N. Hould and K. Majnouka for help and suggestions during the course of the investigation, N. Menagazzo for help with the Raman scans, R. Opila, C. Weiland and Fang Fang for training sessions on the XPS, N. Lorenzo for help with Ar sputtered AES analysis, A. Robinson and P. McNeely for time on the PL equipment and C. Ni and F. Kriss of the W.M. Keck Electron Microscopy Facility at the University of Delaware for providing the scanning electron microscope time and help. Funding for this research was provided by the US Department of Energy Basic Energy Sciences under Grant No. DE-FG02-07ER15921 and DE-FG02-99ER14998.

Appendix A. Supplementary material

Supplementary data associated with this article can be found, in the online version, at doi:10.1016/j.jcat.2011.04.014.

References

[1] M.D. Hernandez-Alonso, F. Fresno, S. Suarez, J.M. Coronado, Energy Environ. Sci. 2 (2009) 1231.
[2] A. Fujishima, K. Honda, Nature 238 (1972) 37.
[3] G. Liu, L. Wang, H.G. Yang, H.-M. Cheng, G.Q. Lu, J. Mater. Chem. 20 (2010) 831.
[4] R. Asahi, T. Morikawa, T. Ohwaki, K. Aoki, Y. Taga, Science 293 (2001) 269.
[5] E.P. Reddy, B. Sun, P.G. Smirniotis, J. Phys. Chem. B 108 (2004) 17198; A. Kubacka, M. Fernández-García, G. Colón, J. Catal. 254 (2008) 272.
[6] M. Anpo, M. Takeuchi, J. Catal. 216 (2003) 505.
[7] K. Nagaveni, M.S. Hegde, G. Madras, J. Phys. Chem. B 108 (2004) 20204.
[8] A. Kudo, K. Omori, H. Kato, J. Am. Chem. Soc. 121 (1999) 11459; M. Oshikiri, M. Boero, J. Ye, Z. Zou, G. Kido, J. Chem. Phys. 117 (2002) 7313.
[9] J. Tang, Z. Zou, J. Ye, Angew. Chem. Int. Edit. 43 (2004) 4463.
[10] Y. Hosogi, H. Kato, A. Kudo, J. Phys. Chem. C 112 (2008) 17678.
[11] Y. Hosogi, H. Kato, A. Kudo, Chem. Lett. 35 (2006) 578; Y. Hosogi, Y. Shimodaira, H. Kato, H. Kobayashi, A. Kudo, Chem. Mater. 20 (2008) 1299; Y. Hosogi, K. Tanabe, H. Kato, H. Kobayashi, A. Kudo, Chem. Lett. 33 (2004) 28.
[12] J. Yu, S. Liu, M. Zhou, J. Phys. Chem. C 112 (2008) 2050.
[13] X. Li, R. Xiong, G. Wei, J. Hazard. Mater. 164 (2009) 587.
[14] J. Lin, J.C. Yu, D. Lo, S.K. Lam, J. Catal. 183 (1999) 368.
[15] M.H. Harunsani, F.E. Oropeza, R.G. Palgrave, R.G. Egdell, Chem. Mater. 22 (2010) 1551.
[16] R. Sui, J.L. Young, C.P. Berlinguette, J. Mater. Chem. 20 (2010) 498.
[17] F. Fresno, J.M. Coronado, D. Tudela, J. Soria, Appl. Catal. B 55 (2005) 159; F. Fresno, C. Guillard, J.M. Coronado, J.-M. Chovelon, D. Tudela, J. Soria, J.-M. Herrmann, J. Photochem. Photobiol. A 173 (2005) 13; F. Fresno, D. Tudela, A.J. Maira, F. Rivera, J.M. Coronado, J. Soria, Appl. Organomet. Chem. 20 (2006) 220.
[18] F. Fresno, D. Tudela, J.M. Coronado, M. Fernandez-Garcia, A.B. Hungria, J. Soria, Phys. Chem. Chem. Phys. 8 (2006) 2421.
[19] A. Weibel, R. Bouchet, S.L.P. Savin, A.V. Chadwick, P.E. Lippens, M. Womes, P. Knauth, ChemPhysChem 7 (2006) 2377.
[20] R. Long, Y. Dai, B. Huang, J. Phys. Chem. C 113 (2008) 650.
[21] F.R. Sensato, R. Custodio, E. Longo, A. Beltrán, J. Andrés, Catal. Today 85 (2003) 145.
[22] F. Sayllkan, M. Asiltürk, P. Tatar, N. Kiraz, S. Sener, E. Arpaç, H. Sayllkan, Mater. Res. Bull. 43 (2008) 127.
[23] Y. Cao, W. Yang, W. Zhang, G. Liu, P. Yue, New J. Chem. 28 (2004) 218.
[24] M. Ghosh, V. Pralong, A. Wattiaux, A. Sleight, M. Subramanian, Chem. – Asian J. 4 (2009) 881.
[25] D.R. Li, L.N. Sun, C.W. Hu, Chin. Chem. Lett. 17 (2006) 1089.
[26] H. Uchiyama, H. Imai, Chem. Commun. (2005) 6014.
[27] S. Mahanty, S. Roy, S. Sen, J. Cryst. Growth 261 (2004) 77.
[28] E.A. Davis, N.F. Mott, Philos. Mag. 22 (1970) 903; X. Gao, I.E. Wachs, J. Phys. Chem. B 104 (2000) 1261.
[29] M.J. Nash, S. Rykov, R.F. Lobo, D.J. Doren, I. Wachs, J. Phys. Chem. C 111 (2007) 7029.
[30] http://www.mcrals.info/.; J. Jaumot, R. Gargallo, A. de Juan, R. Tauler, Chemom. Intell. Lab. Syst. 76 (2005) 101.
[31] R2007a.
[32] V.B. Ram Boppana, D.J. Doren, R.F. Lobo, J. Mater. Chem. 20 (2010) 9787.

[33] K.-i. Ishibashi, A. Fujishima, T. Watanabe, K. Hashimoto, Electrochem. Commun. 2 (2000) 207;
W.A. Armstrong, R.A. Facey, D.W. Grant, W.G. Humpreys, Can. J. Chem. 41 (1963) 1575.
[34] J. Li, H.C. Zeng, J. Am. Chem. Soc. 129 (2007) 15839.
[35] K.-R. Zhu, M.-S. Zhang, Q. Chen, Z. Yin, Phys. Lett. A 340 (2005) 220;
C.Y. Xu, P.X. Zhang, L. Yan, J. Raman Spectrosc. 32 (2001) 862.
[36] W.F. Zhang et al., J. Phys. D: Appl. Phys. 33 (2000) 912;
D. Bersani, P.P. Lottici, T. Lopez, X.-Z. Ding, J. Sol–Gel Sci. Technol. 13 (1998) 849.
[37] S. Brunauer, L.S. Deming, W.E. Deming, E. Teller, J. Am. Chem. Soc. 62 (1940) 1723.
[38] K.S.W. Sing E.D.H., R.A.W. Haul, L. Moscou, R.A. Pierotti R.J., T. Siemieniewska, Pure Appl. Chem. 57 (1985) 603.
[39] Y. Cao, T. He, L. Zhao, E. Wang, W. Yang, Y. Cao, J. Phys. Chem. C 113 (2009) 18121.
[40] T. Omata, M. Kita, S. Otsuka-Yao-Matsuo, M. Katada, J. Phys. Chem. Solids 66 (2005) 53.
[41] H. Xu, Z. Zheng, L. Zhang, H. Zhang, F. Deng, J. Solid State Chem. 181 (2008) 2516.
[42] H. Deng, J.M. Hossenlopp, J. Phys. Chem. B 109 (2004) 66.
[43] T. Watanabe, T. Takizawa, K. Honda, J. Phys. Chem. C 81 (1977) 1845.
[44] C. Zhang, Y. Zhu, Chem. Mater. 17 (2005) 3537.
[45] F. Chen, J. Zhoa, H. Hidaka, Int. J. Photoenergy 5 (2003) 209.
[46] J. Zhuang, W. Dai, Q. Tian, Z. Li, L. Xie, J. Wang, P. Liu, X. Shi, D. Wang, Langmuir 26 (2010) 9686.
[47] T. Wu, G. Liu, J. Zhao, H. Hidaka, N. Serpone, J. Phys. Chem. B 102 (1998) 5845.
[48] Q. Wang, C. Chen, D. Zhao, W. Ma, J. Zhao, Langmuir 24 (2008) 7338.
[49] P. Qu, J. Zhao, T. Shen, H. Hidaka, J. Mol. Catal. A: Chem. 129 (1998) 257.
[50] T. Hirakawa, Y. Nosaka, Langmuir 18 (2002) 3247.
[51] K. Rajeshwar, M.E. Osugi, W. Chanmanee, C.R. Chenthamarakshan, M.V.B. Zanoni, P. Kajitvichyanukul, R. Krishnan-Ayer, J. Photochem. Photobiol. C 9 (2008) 171.
[52] Even if we assume all the tin present as a surface layer of SnO, then its thickness is from 0.18 Å (for Ti/Sn = 50) to 1.75 Å (for Ti/Sn = 5). These values were obtained using the formula, thickness = volume of SnO/BET surface area, per gram of particle.
[53] H. Jianhui, D. Kaining, H. Yidong, W. Xinchen, F. Xianzhi, ChemSusChem 1 (2008) 1011.
[54] The band at ~400 nm corresponding to the band gap of anatase is not observed for Sn^{2+} doped catalysts but is for the calcined Sn^{4+} anatase product Y.-F. Tu, S.-Y. Huang, J.-P. Sang, X.-W. Zou, J. Alloys Compd. 482 (2009) 382.
[55] W. Kallel, S. Bouattour, A.W. Kolsi, J. Non-Cryst. Solids 352 (2006) 3970.
[56] H.E. Chao, Y.U. Yun, H.U. Xingfang, A. Larbot, J. Eur. Ceram. Soc. 23 (2003) 1457.
[57] For the Ti/Sn = 9 ($SnCl_2$) material, quantification (AES) after 3 cycles of sputtering gave a Ti/Sn of 8.8 compared with its surface ratio of 1.87 (XPS).
[58] P.A. Cox, R.G. Egdell, C. Harding, W.R. Patterson, P.J. Tavener, Surf. Sci. 123 (1982) 179.
[59] A. Dieguez, A. Romano-Rodriguez, A. Vila, J.R. Morante, J. Appl. Phys. 90 (2001) 1550.
[60] Q.-H. Wu, J. Song, J. Kang, Q.-F. Dong, S.-T. Wu, S.-G. Sun, Mater. Lett. 61 (2007) 3679.
[61] C.L. Lau, G.K. Wertheim, J. Vac. Sci. Technol. 15 (1978) 622;
M. Kwoka, L. Ottaviano, M. Passacantando, S. Santucci, G. Czempik, J. Szuber, Thin Solid Films 490 (2005) 36.
[62] J.M. Thomas, M.J. Tricker, J. Chem. Soc., Faraday Trans. 2: Mol. Chem. Phys. 71 (1975) 329.
[63] M. Minella, M.G. Faga, V. Maurino, C. Minero, E. Pelizzetti, S. Coluccia, G. Martra, Langmuir 26 (2009) 2521.
[64] M. Primet, P. Pichat, M.V. Mathieu, J. Phys. Chem. C 75 (1971) 1216.
[65] K. Yu, S. Yang, H. He, C. Sun, C. Gu, Y. Ju, J. Phys. Chem. A 113 (2009) 10024.
[66] G. Liu, P. Niu, C. Sun, S.C. Smith, Z. Chen, G.Q. Lu, H.-M. Cheng, J. Am. Chem. Soc. 132 (2010) 11642.
[67] M. Andersson, L. Österlund, S. Ljungström, A. Palmqvist, J. Phys. Chem. B 106 (2002) 10674.
[68] A. Sobczynski, L. Duczmal, W. Zmudzinski, J. Mol. Catal. A: Chem. 213 (2004) 225.
[69] X. Li, C. Chen, J. Zhao, Langmuir 17 (2001) 4118.
[70] F. Fresno, D. Tudela, J.M. Coronado, J. Soria, Catal. Today 143 (2009) 230.
[71] S.K. Kulshreshtha, R. Sasikala, V. Sudarsan, J. Mater. Chem 11 (2001) 930.